Tumor Microenvironment Interaction-Guided Graph Neural Networks for Survival Prediction from Whole-Slide Pathology Images

Dr. Ohmini Krishnamurthy Rajendran
Consultant, MBBS, MD Radiodiagnosis, KIMS Hospital and Research Centre
Krishna Rajendra Road , Parvathipuram, Vishweshwarapura, Basavanagudi, Bengaluru, Karnataka 560004
Jsmnk4@gmail.com

ABSTRACT
Using whole-slide abnormal images, recently developed deep learning technology may help pathologists predict patient survival. Most approaches primarily sampled patches in specified or random tumour regions of WSIs, which restricted their ability to capture the intricate interactions between cancer and micro-environment components. Because the heterogeneous tumour micro-environment (TME) supports and nurtures tumors, it is essential to comprehend cancer formation to study TME and its relationship to tumors. A Tumour Micro-environment Interactions Guided Graph Learning (TMEGL) algorithm based on the spatial interactions between the tumor and its two main components, lymphocytes and stromal fibrosis, was our proposal for human cancer prognosis. First, we built graphs for each WSI using various patch types as nodes. To learn node representations that preserve information about topological structure, a brand-new TME neighbourhood organization driven graph embedding strategy was then suggested. Finally, to predict clinical outcomes, a Gated Graph Attention Network records interactions associated with survival between TME components and tumors. TMEGL was verified on three TCGA cancer cohorts. The results of the experiments show that survival predictions made by the TMEGL model can be explained, making it superior to WSI-based survival analysis methods.

Keywords: *Graph Neural Networks (GNNs), Tumor Microenvironment (TME), Cancer Informatics , Spatial Transcriptomics , Deep Learning in Oncology , Graph Learning*
How to cite this article: Rajendran OK. Tumor Microenvironment Interaction-Guided Graph Neural Networks for Survival Prediction from Whole-Slide Pathology Images. Int J Drug Deliv Technol. 2026;16(49s): 481-488. DOI: 10.25258/ijddt.16.49s.50

I. INTRODUCTION

Cancer threatens human health and quality of life. By 2040, there are expected to be 28.4 million new cases of cancer. As a result, accurate predictions of clinical outcomes, such as survival time, are essential for assisting physicians in the early development of individualized treatment plans. Over the last decade, image-based technologies have shown considerable promise in healthcare research. Because they depict cell morphology and progression, whole-slide pathological images (WSIs) are the industry standard for diagnosing and predicting human cancer. Since pathologists' inter-observational differences are high due to the heterogeneous patterns in WSIs, machine learning techniques are needed to help them predict the likelihood that humans will survive cancer. With the fast growth of deep learning technology, developing WSI-based deep learning models for cancer survival analysis is popular[1]. Deep learning algorithms may automatically learn survival-associated representations from WSIs to enhance prognosis outcomes, unlike typical survival analysis methods that need feature engineering. It is impractical to directly feed WSIs into a deep neural network for model training due to their typically large dimensions (such as 100,000 by 100,000 pixels). To address the aforementioned issues, current research focuses on patch-level and WSI-level annotation strategies. Before using the patch-level annotation approaches for deep model training, professionals must annotate crucial patches like the WSI tumor patches. When multiple WSIs need to be labeled, pathologists must manually annotate patches before selecting them, which is difficult. In order to lessen annotation load, additional methods that only require WSI-level annotations are being developed. Patches are treated as instances by the WSI-level annotation techniques. Using a pooling or attention approach, multi-instance learning (MIL) methods combine patch-level representations to predict WSI targets. Graph convolutional networks, in addition to MIL methods, may be able to learn the global representation of WSIs and provide accurate predictions[2]. Even though a lot of progress has been made, the selected patches are either randomly generated or taken from WSI tumor regions, so the current studies are unable to capture the intricate interactions between the components of the microenvironment and the tumor. It is well acknowledged that cancer is caused by unrestricted tumour cell proliferation and the tumour micro environment (TME), which is mostly stromal fibrosis and lymphocytes. Numerous interactions between tumor and stromal fibrosis speed up tumor progression by facilitating tumor invasion and metastasis, while the major interactions between lymphocytes and tumors reduce survival risk due to the immune system's ability to regulate tumor growth through activation of adaptive and innate immune mechanisms. Better outcomes should be expected from the prognosis model if tumor-TME crossings are included. We know of no WSI-based graph learning methods that used a ready-made, pre-trained network like ResNet101 or VGG16 to directly extract node attributes from selected patches. However, these node representations failed to take into account the TME topology, which has been linked to cancer[3]. Thus, this research suggested a Tumour Micro-environment Interactions Guided

Graph Learning (TMEGL) approach for cancer prognosis prediction. Three factors describe this study's key contribution:

- We created TMEGL, a graph learning system for human cancer survival analysis, that combines tumor-TME component interactions (lymphocytes and stromal fibrosis).
- We developed a method for embedding graphs that keeps the spatial arrangement of tumor and TME elements out of the graph domain.
- To predict WSI survival, we developed gated graph attention networks (GGATs).
- While graph attention layers characterize node intersections, gated graph convolution layers update the node representation from nearby nodes of the same type.

II. RELATED WORK

A. Analyze WSIs based on Patch-level Annotation

Pathologists were required to select multiple patches for patch-level annotation approaches to indicate cancer aggressiveness for model training. Using selected patches from WSIs, the research has developed computational pipelines to extract hand-crafted characteristics for diagnosis and prognosis. A number of patch-level methodologies have been incorporated into deep neural network frameworks as a result of deep learning's success. Zhu et al. proposed the first deep CNN model for predicting patient survival based on pathology age. A Delaunay triangulation network and a deep autoencoder were used by Cheng et al. to compare cell-cell interactions in patients with low and high survival risk and learn cell representation from extracted patches. Since there aren't enough annotated patches to train a robust deep learning model, some patch-based methods also used data augmentation or transfer learning to improve human cancer prediction[4].

B. Analyze WSIs based on WSI-level Annotation

WSI-level methods only use WSI annotations to analyze abnormal images, whereas patch-level algorithms require extensive pathologist annotation. The multi instance learning (MIL) framework, which treats WSIs as bags and instances as patches sampled from them, is utilized by the majority of WSI-level approaches. Global pooling techniques for patch-based instances that effectively aggregate patch-level data to WSI-level representations were developed as part of the study. For WSI classification, Li et al. presented a dual stream multiple instance learning network, and Chen et al. presented a Transformer-based method for location-based analysis of human cancer survival. In addition to the MIL framework, some studies used the spatial structure of extracted patches and the graph convolutional network (GCN) to predict cancer patient outcomes. Pre-trained networks or information about the graph structure were used in these graph learning methods to represent nodes, which limited their ability to reveal the topological architecture of the cancer microenvironment for survival prediction[5].

III. METHOD

Our four-step technique design is depicted in Fig. 1. As nodes, we initially constructed a graph by extracting tumor, lymphocyte, and stromal fibrosis image patches from each WSI. We then examined each node's TME structure and created a TME neighbourhood organization guided graph embedding technique to learn node representations. Utilizing learned node embeddings, the gated graph attention net (GGAT) depicts intersections of tumor-TME components. Finally, survival is predicted by the Cox model[6].

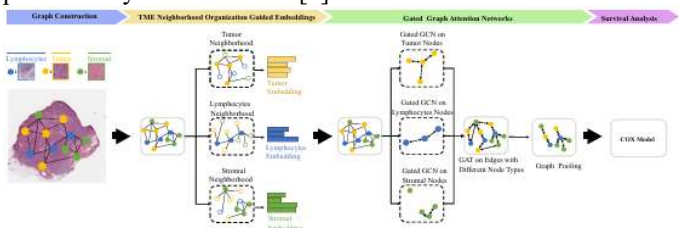

Figure 1. The suggested technique TMEGL flowchart For graphing, lymphocyte, tumour, and stromal patches are isolated from the whole-slide pathological picture. Second, retrieved patches are used to teach a cancer micro-environment organization-guided network embedding method node representations. Third, we model node type intersections using a gated graph attention network. Finally, survival is predicted by the Cox model.

A. WSI Pre-processing and Graph Construction

All gathered WSIs are big (e.g., 100Kx100K pixels). To begin, we split it into 512x512 non-overlap patches. Since the created patches may not contain sufficient tissues, we selected patches with image densities greater than 0.7 for further investigation. Picture density is calculated here as the proportion of pixels in that area that are not white (at least one red, green, and blue value is below 200 in 24 bit RGB color space). Using the annotated dataset from, we then trained a U-net++ network to semantically divide the lymphocyte, stromal, and tumor areas in each patch. The tissue segmentation model's ability to achieve a dice ratio of 0.858, as demonstrated by our investigation and testing, calls for further investigation[7]. We estimated the cancer, lymphocyte, and stromal area ratios for each valid patch at the pixel level, then selected the 300 patches with the highest ratios for each patch type. We made a graph for each WSI from patches of the tumor, lymphocyte, and stroma. We regarded patches as nodes and used the K-closest Neighbours (KNN) technique to form the graph by computing Euclidean distances between pairs of patches with 50 closest neighbours per node[8].

B. TME Neighborhood Organization Guided Graph Embedding for Nodes Representations

The majority of studies used pre-trained networks like ResNet-101 and VGG-16 to represent the node in the graph of each patch. Based on the organization of the tumor micro-environment (TME), which is known to influence cancer growth in humans, these feature extraction algorithms are unable to measure node similarity. A cancer zone surrounded by tumor-infiltration lymphocytes will have a better probability of presenting an immune response to inhibit tumour growth, therefore its representation should vary from ordinary tumour patches[9]. Because stromal tissues are immunosuppressive during cancer growth, two lymphocyte patches surrounded by stromal fibrosis should have identical representations in another scenario. We presented a neighbourhood organization driven

graph embedding method to learn the unique representation of each node type in TME in order to maintain topological similarity. Lymphocytes and stromal nodes can be easily included in this graph embedding technique that was demonstrated on cancer nodes (Fig. 2). Let vM 1, vM 2,..., vM 300 represent the 300 tumor nodes in WSI's graph G. We looked for similarities between their TME neighborhood organizations[10]. This is vM_i$'s TME organization with k-hop:

$$(q_i^M)^k = [\frac{(N_i^M)^k}{(N_i)^k}, \frac{(N_i^L)^k}{(N_i)^k}, \frac{(N_i^R)^k}{(N_i)^k}] \quad (1)$$

(NM i)k, (NL i)k, and (NR i)k are the proportions of TME components that can characterize the topological organization of vM i, and (Ni)k is the number of nodes k-hop away. (qM i)k is the number of tumor, lymphocyte, and stromal nodes in the k-hop neighborhood of xM i. To characterize TME spatial structure at a variety of distance levels, we used TME neighbourhood information from 1-, 2-, and 3-hop hop ranges to represent each node in this study:

$$q_i^M = [(q_i^M)^1, (q_i^M)^2, (q_i^M)^3] \quad (2)$$

The tumor nodes vM i and vM j's TME organization similarity can then be calculated:

$$s(v_i^M, v_j^M) = \frac{q_i^M (q_j^M)^T}{\|q_i^M\| \, \|q_j^M\|} \quad (3)$$

Based on pairwise similarity, we clustered all tumour nodes into B groups using the spectral clustering technique. The t-th group's components include:

$$P_t^M = \{P_{t1}^M, P_{t2}^M, ...P_{t|P_t^M|}^M\}, t = 1, 2, ..., B \quad (4)$$

where PM t is a cardinal. The sample in the -th group with the highest average similarity to PM t samples is the centroid nodePM tc. The intra-group similarity vector (So t)tra∈R|PM t |−1 was determined using clustering findings. It might compare the neighborhood arrangement of the centroid node to the other components of PM t:

$$(S_t^o)^{tra} = norm([s(P_{t1}^M, P_{tc}^M), ..., s(P_{t|P_t^M|}^M, P_{tc}^M)]) \quad (5)$$

The vector is normalized using the norm(.) operation to ensure that its total is 1. We also calculated centroid node similarities to determine inter-group similarity among generated B groupings. The following is the definition of the intergroup similarity vector for the t-th group (So t) terRB1:

$$(S_t^o)^{ter} = norm([s(P_{1c}^M, P_{tc}^M), ..., s(P_{Bc}^M, P_{tc}^M)]) \quad (6)$$

The embedding network was used to calculate the tumor nodes' intra- and inter-group similarity (Se t)tra and ter) based on the graph domain clustering results (Eq. (4)). Kullback–Leibler (KL) divergence on Bgroups is the goal loss function: to train node embeddings that retain the graph-retrieved TME organization similarity,

$$L = \sum_{t=1}^{B} KL((S_t^e)^{tra}, (S_t^o)^{tra}) + \lambda((S_t^e)^{ter}, (S_t^o)^{ter}) \quad (7)$$

We optimise the aim in Eq. (7) to get TME organization embeddings, preserving intra-group and inter-group similarity information. The regularisation value λ may be adjusted using cross validation. The TME neighbourhood organisation guided graph embedding technique may also create representations for additional nodes.

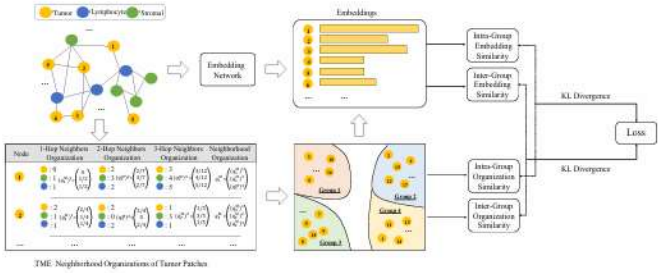

Figure 2. Proposed TMENeighborhood Organization Scheme with Guided Graph Embedment on Tumour Nodes

C. Gated Graph Attention Networks for Survival Analysis of Human Cancers

Similar TME components interact with one another to change their status [12]. Cancer prognosis depends heavily on TME component interactions. In light of this, we propose a Gated Graph Attention Network with GGC and GAT layers to record TME component interactions[11].

given patches for each WSI-based graph G's vertices. The Tumor, Lymphocytes, and Stromal sub-graphs of G are represented by GM, GL, and GR. Gated Graph Convolution Layer updates node representations from nearby nodes of the same type using learned node embeddings dw i Rd(i = 1,2,...300) in each sub-graph. All of the nodes in Gw(w in M,L,R) are of the same type.

$$\begin{aligned} (h_i^w)^0 &= d_i^w||0 \\ (a_i^w)^t &= \sum_{j \in N(i)} u_{ij} (h_j^w)^t \\ (h_i^w)^{t+1} &= GRU((a_i^w)^t, (h_i^w)^t) \end{aligned} \quad (8)$$

(hw i)0 R2d is initialized according to Eq.(8) by copying node embeddings into its first components and padding the rest with zeros. Using information from nearby nodes j N(i) with weight uij and the previous step, the subsequent GRU-like updates update nodes i. The GAT layer for node interaction follows next. GAT layer inputs are H = [HM,HL,HR] ∈ Rd×900, whereas Hw = [hw 1,hw 2,...,hw 300] ∈ Rd× 300, w ∈ {M,L,R} represents output characteristics for each node type following GGC layer. Using the linear transform matrix T Rdd′ and (Hw)′ Rd′ 300, w M,L,R, the GAT layer generates new node features H ′ = [(HM)′, (HL)′, (HR)′]. The normalised attention coefficients between nodes i with type w and node j with type z are calculated using a shared attention mechanism Rd′ × Rd′ → R:

$$e_{ij}^{w,z} = a(Th_i^w, Th_j^z), w \neq z \quad (9)$$

Using Softmax, GAT normalizes the values of node j eij:

$$\alpha_{ij}^{w,z} = \frac{\exp(e_{ij}^{w,z})}{\sum_{\substack{j\in N_i \\ v\neq w}} exp(e_{ij}^{w,v})} \quad (10)$$

Where Ni is the neighbors of node i. The output characteristic of each node after the GAT layer is:

$$h_i^w = \sigma(\sum_{\substack{j\in N_i \\ w\neq z}} \alpha_{ij}^{w,z} T h_j^z) \quad (11)$$

Eq. (11) states that while the GGC layer transfers information between nodes of the same type, the GAT layer records interactions between distinct nodes. We utilized SAGPooL to identify the highest s(s in [0,100]) percentage of nodes with high attention ratings in order to avoid overfitting and identify survival-related interactions of TME components[12]. The last layer of GAT uses a global attention pooling approach to combine node characteristics into WSI-level features for survival analysis. In this study, we analyzed human cancer survival using the widely used Cox proportional hazard model. Performance of the survival analysis model is measured by the AUC and the Concordance Index (CI). Higher CI and AUC values (0–1) are associated with improved prognoses[13].

D. Time Complexity Analysis

Three components dominate TMEGL complexity if a graph has n nodes for each node type. The difficulty of calculating node sim ilarity within one node type is O(n2d), where d is the embedding dimension. Second, the spectral clustering technique for grouping nodes into g clusters is $O(n^3)$ difficult. Finally, we use O(g2) to calculate similarities between groups. O(n2d+n3 + g2) is the TMEGL's temporal complexity. Despite the difficulty of spectral clustering, we set n to 300 in order to optimize computations[14]..

IV. EXPERIMENTAL RESULTS

A. Dataset

The Cancer Genome Atlas (TCGA) cohorts BRCA, KIRC, and LUSC were used for our investigations. The demographics of these three cancer cohorts are shown in Table 1:

Table 1. Clinical and demographic data.

Dataset	Patient Count	Mean Age (Years)	Follow-up Time (Months)	Censored	Non-censored
KIRCUS	690	54.6	25.3	627	63
BRCA	511	66.17	31.8	340	171
Dataset 3	472	59.20	36.1	270	202

B. Experimental Settings

For each cancer cohort, method performance is evaluated using 5-fold cross validation. Validation samples for parameter adjustment are randomly picked from the training dataset at 25%. Pre-trained ResNet-101 is used to extract node features and feed them into the embedding network to create 128-dimensional node embeddings for the graph embedding method described in Section 3.2. The embedding network is made up of two completely linked, 512- and 128-dimensional layers. Equation (7) demonstrates that we use the spectral clustering method to divide the nodes into B = 4 groups and adjust the regularization value from 1 to 1e5 in order to balance the similarities between and within the groups[15]. Gated Graph Attention Networks with three GAT, three GGC, and two graph pooling layers are suggested in Section 3.3. Each of the three GAT layers has 128 dimensions and 1–6 recurring steps. Additionally, each SAGPool layer has 0.3 to 1 saved nodes. Finally, we experimentally establish 200 epochs and tweak the learning rate from 1e-8 to 1e-2.

C. Comparison of TMEGL with Other Survival Analysis Models

Using CI and AUC from Section 3.4, TMEGL was then compared to the following WSI-based survival analysis models. 1) To predict WSI, the ensemble model WSISA combines patch-level deep survival analysis models. A deep multiple instance learning model called DeepAttnMISL teaches gigapixel WSI survival patterns directly. 3) DeepGraphSurv: Attention-learning graph convolutional neural network for WSI survival prediction using topological properties. 4) MCAT: Transformer-based survival prediction utilising WSIs and location information. 5) Patch GCN is a context-aware graph convolutional network that learns WSI global representations by collecting instance-level histological features in a hierarchical fashion. 6) Clu Siam: WSI survival prediction using self-supervised learning (SSL) representation learning. 7) HGSurvNet: A hyper-graph-based WSI survival prediction system and Co-Pilot: a dynamic point-cloud-based WSI representation for cancer survival prediction[16] In terms of predictive power, graph-based deep learning methods like DeepGraphSurv, Patch-GCN, TMEGL, andHGSurvNet outperform multi-instance learning algorithms like WSISA and DeepAttnMISL, as shown in Table 2. This is due to the fact that GCN-based methods combine the topological structure of WSI. Second, our suggested TMEGL can get CI values of 0.719, 0.697, and 0.695 and AUC values of 0.750, 0.716, and 0.736 on BRCA, KIRC, and LUSC populations. Comparing graph learning methods with SOTA WSI-based representation learning algorithms (CluSiam and Co-Pilot) yields significantly inferior results. This is because the proposed TMEGL might take into account the topological arrangement of TMEs, which has been linked to the development of cancer.

Table2. TMEGL and By CI and AUC (with standard deviations), additional models

Method	BRCA CI	BRCA AUC	KIRC CI	KIRC AUC	LUSC CI	LUSC AUC
WSISA [43]	0.621 (0.02)	0.590 (0.05)	0.578 (0.04)	0.607 (0.05)	0.577 (0.04)	0.587 (0.05)
DeepAttnMISL [40]	0.617	0.637	0.629	0.654	0.654	0.677

	(0.05)	(0.04)	(0.05)	(0.03)	(0.04)	(0.03)
MCAT [5]	0.638 (0.05)	0.651 (0.04)	0.631 (0.05)	0.659 (0.05)	0.643 (0.05)	0.679 (0.05)
DeepGraph Surv [18]	0.653 (0.04)	0.665 (0.06)	0.649 (0.04)	0.671 (0.04)	0.651 (0.04)	0.683 (0.03)
Patch-GCN [4]	0.664 (0.04)	0.671 (0.03)	0.662 (0.03)	0.686 (0.03)	0.648 (0.05)	0.687 (0.04)
CluSiam [36]	0.644 (0.07)	0.639 (0.05)	0.667 (0.04)	0.691 (0.02)	0.651 (0.04)	0.671 (0.03)
Co-Pilot [25]	0.657 (0.03)	0.672 (0.03)	0.639 (0.05)	0.661 (0.03)	0.674 (0.03)	0.691 (0.03)
TMEGL	0.719 (0.03)	0.750 (0.03)	0.697 (0.03)	0.716 (0.03)	0.695 (0.04)	0.736 (0.04)
HGSurvNet [8]	0.671 (0.04)	0.681 (0.05)	0.659 (0.04)	0.681 (0.04)	0.701 (0.03)	N/A

D. Comparison of TMEGL with Other Methods for Patient Stratification

The subgrouping of patients for individualized treatment is yet another crucial obstacle in human cancer survival analysis. The retrieved WSI-level characteristics of the patients in the test set were divided into two groups using the K-means clustering method in this study. The log-rank test is used to see if these two groups have significant clinical outcomes. As various methods demonstrate in Fig. 3, a lower log-rank test p-value indicates better prognosis prediction. On BRCA, KIRC, and LUSC datasets, our TMEGL outperforms HGSurvNet and Co-Pilot with p-values of 3.32e2, 2.01e2, and 3.01e3 (Fig. 3). These data once more demonstrate the advantages of our TMEGL method.

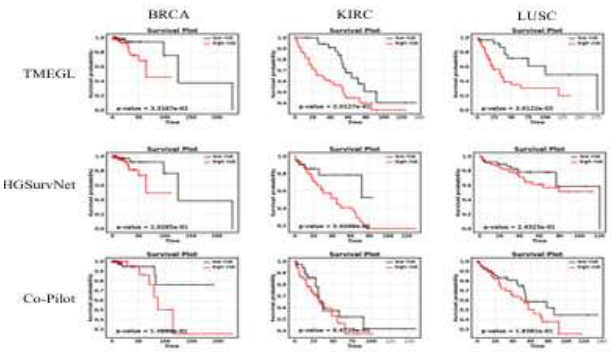

Figure3. Methods' Stratification Performance Comparison

E. The Difference of the Interactions Between High and Low survival Risk Patients

Graph pooling was used to examine the percentage of survival-associated connections linking various organs for stratified individuals on different survival groups in Fig.3. The majority of the BRCA cohort's survival-associated edges are connected to lymphocyte-tumor (L-T) interactions in WSIs, as depicted in Fig.4(a). Furthermore, the low-risk group has more edges connecting lymphocytes and tumor regions than the high-risk group, indicating that the immune system is able to control tumor growth and reduce survival risks. We also discovered that high-survival risk groups had larger Stromal-Tumor(S-T) interaction ratios than low-survival risk groups.Such findings are consistent with the understanding that rich tumor-stromal fibrosis connections increase tumour invasion and metasis, increasing survival risk[17].

We also showed the tumour, lymphocytes, and stromal patches and their boundaries in Fig.4(b). GAT-weighted edges are depicted by the thick black lines. Fig. 4(b) demonstrates that patients with a low survival risk (long survival time) have a higher lymphocyte density than patients with a high survival risk (short survival time), who have more cancer areas. According to these findings, lymphocyte density and patient survival are related. As demonstrated in Fig.4(b), patients in the low-survivalrisk group have more edges linking tumour and TIL areas, whereas those in the high-survivalrisk group have more tumor-stromal connections. The proposed TMEGL's strong explainability for studying TME component associations on the survival prediction task is supported by these findings, which are shown in Fig. 4(a).

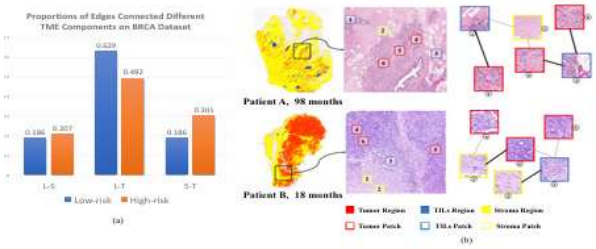

Figure4. (a): Cross-type patch interactions. Thick dark lines indicate graph Attention Network edges with higher weights. (b) Different TME component edge proportions.

F. Ablation Study

In order to evaluate TMEGL's performance, its variations were compared to the average Concordance Index (CI) value in the five-fold cross validation. 1) Survival prediction was made directly using gated graph attention networks without the need for graph embedding. TMEGL-DW trained survival prediction node embeddings using Deepwalk. TMEGL-GAT: used the GAT directly to record node interactions regardless of edge type. TMEGL-N1 and N2 consider 1-hop and 2-hop neighbourhood organization for the graph-embedding procedure. TMEGL-G2 and TMEGL-G5: To compute intra-group and inter-group similarity for graph embedding learning, each kind of node is grouped into B = 2 and B = 5 groups. 6) TMEGL-Inter and TMEGL-Intra: Using only intra- or inter-

group similarity to learn node embeddings Table 3 contains the results of the experiment. According to Table 3, the TME neighborhood organization guided graph embedding method that has been proposed performs better than TMEGL-NE and TMEGL-DW[18]. TMEGL also outperforms TMEGL-GAT, suggesting that considering edges with similar or different nodes might improve prognosis.Since it characterises the TME structure across a greater hop range, TMEGL is more prognostic than TMEGL-N1 and N2. Next, if the group number is low (TMEGL-G2) for learning graph embeddings, the TMEGL prognosis results will be significantly reduced. Our findings will remain constant as group size increases (TMEGL-G5) because the tiny group number may not reflect the commonalities between and within the groups on the graph. Last but not least, TMEGL outperformed TMEGL-Intra and TMEGL-Inter, indicating that learning node embeddings using information about similarity between and within groups can improve prognoses.

Table3. TMEGL and variations in CI measurement comparison.

Method	BRCA	KIRC	LUSC
TMEGL	0.719	0.697	0.695
TMEGL-NE	0.609	0.629	0.618
TMEGL-DW	0.658	0.631	0.621
TMEGL-GAT	0.662	0.630	0.633
TMEGL-N1	0.644	0.641	0.634
TMEGL-N2	0.671	0.663	0.657
TMEGL-G2	0.643	0.633	0.641
TMEGL-G5	0.694	0.680	0.681
TMEGL-Intra	0.676	0.636	0.641
TMEGL-Inter	0.668	0.623	0.646

V. CONCLUSION

TMEGL is a unique WSI-based survival prediction model for human cancer prognosis. To our knowledge, TMEGL is the first prospective research to predict patient outcomes using tumor-TME interactions. Experiments also demonstrate that the proposed strategy works. In conclusion, TMEGL is a WSI-based generic graph learning framework that enables individualized treatment by predicting cancer survival and explaining tumor growth. With less annotated data for pre-selecting key WSI patches, we propose constructing an accurate segmentation model through active learning and semi-supervised learning.

VI. REFERENCES

[1]. Richard J Chen, Ming Y Lu, Muhammad Shaban, Chengkuan Chen, Tiffany Y Chen, Drew FK Williamson, and Faisal Mahmood. Whole slide images are 2d point clouds: Context-aware survival prediction using patch-based graph convolutional networks. In In Proceedings of Medi cal Image Computing and Computer Assisted Intervention, pages 339–349. Springer, 2021.

[2]. Richard J Chen, Ming Y Lu, Wei-Hung Weng, Tiffany Y Chen, Drew FK Williamson, Trevor Manz, Maha Shady, and Faisal Mahmood. Multimodal co-attention transformer for survival prediction in gigapixel whole slide images. In Proceedings of the IEEE/CVF International Conference on Computer Vision, pages 4015–4025, 2021.

[3]. Jun Cheng, Zhi Han, Rohit Mehra, Wei Shao, Michael Cheng, Qianjin Feng, Dong Ni, Kun Huang, Liang Cheng, and Jie Zhang. Computational analysis of pathological im ages enables a better diagnosis of tfe3 xp11. 2 translocation renal cell carcinoma. Nature Communications, 11(1):1778, 2020.

[4]. Dr. Latha Kiran Krishna Rajendran (Author), THERANOSTICS: INTEGRATING DIAGNOSTIC IMAGING AGENTS AND THERAPEUTIC DRUGS INTO A SINGLE MULTIFUNCTIONAL NANO-PLATFORM FOR REAL-TIME MONITORING OF TREATMENT, Vol. 53 No. 2 (2025): April-June 2025, Power System Protection and Control, ISSN-1674-3415, https://pspac.info/index.php/dlbh/article/view/305 , DOI: https://doi.org/10.46121/pspc.53.2.31

[5]. Rajendran, O. K. (2025). Digital twin frameworks for personalized cancer progression modeling using Longitudinal data. Power System Protection and Control, 53(4), 486–501. https://doi.org/10.46121/pspc.53.4.33

[6]. N. Le, V. S. Rathour, K. Yamazaki, K. Luu, and M. Savvides, "Deep reinforcement learning in computer vision: A comprehensive survey," Artificial Intelligence Review, pp. 1–87, 2022

[7]. Hemanth Kumar, R. M. (2026). Integrated transcriptomic and machine learning framework identifies A blood-based biomarker signature for anthracycline-induced cardiotoxicity in juvenile cancer Survivors. International Journal of Drug Delivery Technology, 16(40s), 219–230. https://doi.org/10.25258/ijddt.16.40s.24

[8]. Rajendran, O. K. (2025). Deep learning for cross-modality mapping between histopathology and radiological imaging. Power System Protection and Control, 53(3), 313–328.https://doi.org/10.46121/pspc.53.3.21

[9]. G. Dulac-Arnold, N. Levine, D. J. Mankowitz, J. Li, C. Paduraru, S. Gowal, and T. Hester, "Challenges of real-world reinforcement learning: Definitions, benchmarks and analysis," Machine Learning, vol. 110, no. 9, pp. 2419–2468, 2021.

[10]. Dr. Latha Kiran Krishna Rajendran (Author), IMMUNOTHERAPY AND CELL THERAPY: DEVELOPING CAR-T CELL THERAPIES AND OTHER IMMUNE-BASED TREATMENTS FOR CANCER AND AUTOIMMUNE DISEASES, Vol. 51 No. 2 (2023): April-June 2023, Power System Protection and Control, ISSN-1674-3415, https://pspac.info/index.php/dlbh/article/view/304 , DOI:https://doi.org/10.46121/pspc.51.2.7

[11]. S. K. Zhou, H. Greenspan, C. Davatzikos, J. S. Duncan, B. Van Ginneken, A. Madabhushi, J. L. Prince, D. Rueckert, and R. M. Summers, "A review

of deep learning in medical imaging: Imaging traits, technology trends, case studies with progress highlights, and future promises," Proceedings of the IEEE, vol. 109, no. 5, pp. 820–838, 2021.

[12]. Dr. Latha Kiran Krishna Rajendran (Author), STRICT LIABILITY OR FAULT-BASED REGIMES FOR AI-CAUSED HARM? A DOCTRINAL ANALYSIS ACROSS COMMON LAW AND CIVIL LAW SYSTEMS, Vol. 52 No. 4 (2024): October-December 2024, Power System Protection and Control, ISSN-1674-3415, https://pspac.info/index.php/dlbh/article/view/312, DOI:https://doi.org/10.46121/pspc.52.4.13

[13]. H. Sung, J. Ferlay, R. L. Siegel, M. Laversanne, I. Soerjomataram, A. Jemal, and F. Bray, "Global cancer statistics 2020: Globocan estimates of incidence and mortality worldwide for 36 cancers in 185 countries," CA: a cancer journal for clinicians, vol. 71, no. 3, pp. 209–249, 2021.

[14]. Dr. Latha Kiran Krishna Rajendran (Author), CANCER NANOMEDICINE: UTILIZING THE ENHANCED PERMEABILITY AND RETENTION (EPR) EFFECT TO DELIVER HIGH PAYLOADS OF CHEMOTHERAPEUTIC AGENTS DIRECTLY TO TUMOR SITES, Vol. 52 No. 2 (2024): April-June 2024, Power System Protection and Control, ISSN-1674-3415, https://pspac.info/index.php/dlbh/article/view/311 , DOI:https://doi.org/10.46121/pspc.52.2.12

[15]. Dr. Latha Kiran Krishna Rajendran (Author), MECHANISMS DRIVING IMMUNOTHERAPY RESISTANCE IN COLORECTAL CANCER LIVER METASTASES, Vol. 52 No. 1 (2024): January-March 2024 , Power System Protection and Control, ISSN-1674-3415, https://pspac.info/index.php/dlbh/article/view/303 DOI: https://doi.org/10.46121/pspc.52.1.5

[16]. Rajendran, O. K. (2023). Federated radiology AI models for multi-institutional cancer diagnosis without data sharing. Power System Protection and Control, 51(4), 38–54. https://doi.org/10.46121/pspc.51.4.5

[17]. Rajendran, O. K. (2023). AI-based radiogenomic models for predicting immunotherapy response in Solid tumors. Power System Protection and Control, 51(4), 24–37. https://doi.org/10.46121/pspc.51.4.4

[18]. Rajendran, L. K. K. (2026). Integrative pharmacogenomic analysis of drug response heterogeneity across cancer cell lines: Insights from large-scale GDSC data. Scientific Culture, 12(4), 7537–7546. https://doi.org/10.5281/zenodo.12426762

[19]. R. Van De Schoot, J. De Bruin, R. Schram, P. Zahedi, J. De Boer, F. Weijdema, B. Kramer, M. Huijts, M. Hoogerwerf, G. Ferdinands, et al., "An open source machine learning framework for efficient and transparent systematic reviews," Nature machine intelligence, vol. 3, no. 2, pp. 125–133, 2021.

[20]. Rajendran, O. K. (2024). Foundation model–driven precision oncology: Integrating multi-omics, radiology, and clinical data for predictive cancer care. Power System Protection and Control, 52(2),154–163. https://doi.org/10.46121/pspc.52.2.14

[21]. Rajendran, O. K. (2024). Self-supervised multimodal learning for early cancer detection across Imaging and genomics. Power System Protection and Control, 52(4), 167–178. https://doi.org/10.46121/pspc.52.4.14

[22]. Rajendran, L. K. K. (2026). Evaluating the association of cancer-related risk factors with multisystem health: Insights into fertility, cardiovascular, and renal indicators. Scientific Culture, 12(4), 7520–7527. https://doi.org/10.5281/zenodo.12426760

[23]. Rajendran, L. K. K. (2026). Impact of treatment modalities on fertility, sexual function, and Psychological outcomes in testicular cancer survivors: A comprehensive review. International Journal of Drug Delivery Technology, 16(30s), 447–453. https://doi.org/10.25258/ijddt.16.30s.43

[24]. Rajendran, L. K. K. (2026). From prediction to practice: A machine learning–based clinical decision Support tool for bevacizumab risk stratification in oncology. International Journal of Drug Delivery Technology, 16(30s), 414–429. https://doi.org/10.25258/ijddt.16.30s.40

[25]. Rajendran, L. K. K. (2026). From prediction to precision: An externally validated deep learning–based Survival and adjuvant therapy recommendation system for resected stage III non-small cell lung Cancer. International Journal of Drug Delivery Technology, 16(30), 430–438. https://doi.org/10.25258/ijddt.16.30.41

[26]. Rajendran, L. K. K. (2026). Interpretable machine learning for early mortality prediction in acute Myeloid leukemia: A decision tree–based retrospective cohort study. International Journal of Drug Delivery Technology, 16(40s), 231–241. https://doi.org/10.25258/ijddt.16.40s.25

[27]. Rajendran, L. K. K. (2026). Machine learning–driven symptom-based cancer risk stratification: A Systematic review of clinical prediction models and methodological rigor. International Journal of Drug Delivery Technology, 16(40s), 242–253. https://doi.org/10.25258/ijddt.16.40s.26

[28]. S. K. Zhou, H. N. Le, K. Luu, H. V. Nguyen, and N. Ayache, "Deep reinforcement learning in medical imaging: A literature review," Medical image analysis, vol. 73, p. 102 193, 2021.

[29]. Donglin Di, Changqing Zou, Yifan Feng, Haiyan Zhou, Rongrong Ji, Qionghai Dai, and Yue Gao. Generating hypergraph-based high-order

representations of whole-slide histopathological images for survival prediction. IEEE Transactions on Pattern Analysis and Machine Intelligence, 45(5):5800–5815, 2022.

[30]. Kevin W Eliceiri. Dual-stream multiple instance learn ing network for whole slide image classification with self supervised contrastive learning. In Proceedings of the IEEE/CVF conference on Computer Vision and Pattern Recognition, pages 14318–14328, 2021.

[31]. Henrik Failmezger. Topological tumor graphs: a graph based spatial model to infer stromal recruitment for immuno suppression in melanoma histology. Cancer research, 80(5): 1199–1209, 2020.

[32]. Tobias Hoch, Daniel Schulz, Nils Eling, Julia Mart´ınez G´omez, Mitchell P Levesque, and Bernd Bodenmiller. Mul tiplexed imaging mass cytometry of the chemokine milieus in melanoma characterizes features of the response to im munotherapy. Science Immunology, 7(70):eabk1692, 2022.

[33]. Sunkyu Kim, Keonwoo Kim, Junseok Choe, Inggeol Lee, and Jaewoo Kang. Improved survival analysis by learning shared genomic information from pan-cancer data. Bioinfor matics, 36(Supplement 1):i389–i398, 2020.

[34]. Nicole M Kuderer, Aakash Desai, Maryam B Lustberg, and Gary H Lyman. Mitigating acute chemotherapy-associated adverse events in patients with cancer. Nature Reviews Clin ical Oncology, 19(11):681–697, 2022.

[35]. Tiancheng Lin, Hongteng Xu, Canqian Yang, and Yi Xu. Interventional multi-instance learning with deconfounded instance-level prediction. In Proceedings of the AAAI Con ference on Artificial Intelligence, pages 1601–1609, 2022.

[36]. MingYLu,DrewFKWilliamson,TiffanyYChe n,RichardJ Chen, Matteo Barbieri, and Faisal Mahmood. Data-efficient and weakly supervised computational pathology on whole slide images. Nature Biomedical Engineering, 5(6):555 570, 2021

[37]. Ramin Nakhli, Allen Zhang, Ali Mirabadi, Katherine Rich, Maryam Asadi, Blake Gilks, Hossein Farahani, and Ali Bashashati. Co-pilot: Dynamic top-down point cloud with conditional neighborhood aggregation for multi-gigapixel histopathology image representation. In Proceedings of the IEEE/CVF International Conference on Computer Vision, pages 21063–21073, 2023.

[38]. Jackson Nyman, Thomas Denize, Ziad Bakouny, Chris Labaki, Breanna M Titchen, Kevin Bi, Surya Narayanan Hari, Jacob Rosenthal, Nicita Mehta, Bowen Jiang, et al. Spatially aware deep learning reveals tumor heterogeneity patterns that encode distinct kidney cancer states. Cell Re ports Medicine, 4(9), 2023.

[39]. Xuejun Qian, Jing Pei, Hui Zheng, Xinxin Xie, Lin Yan, Hao Zhang, Chunguang Han, Xiang Gao, Hanqi Zhang, Weiwei Zheng, et al. Prospective assessment of breast cancer risk from multimodal multiview ultrasound images via clinically applicable deep learning. Nature Biomedical Engineering, 5 (6):522–532, 2021

[40]. Wei Shao, Tongxin Wang, Zhi Huang, Zhi Han, Jie Zhang, and Kun Huang. Weakly supervised deep ordinal cox model for survival prediction from whole-slide pathological im ages. IEEE Transactions on Medical Imaging, 40(12):3739 3747, 2021.

[41]. Mei-Ling Wang, Wei Shao, Xiao-Ke Hao, and Dao-Qiang Zhang. Machine learning for brain imaging genomics meth ods: a review. Machine intelligence research, 20(1):57–78, 2023

[42]. Weiyi Wu, Chongyang Gao, Joseph DiPalma, Soroush Vosoughi, and Saeed Hassanpour. Improving representation learning for histopathologic images with cluster constraints. In Proceedings of the IEEE/CVF International Conference on Computer Vision, pages 21404–21414, 2023.

[43]. Yawen Wu, Yingli Zuo, Qi Zhu, Jianpeng Sheng, Daoqiang Zhang, and Wei Shao. Transfer learning-assisted survival analysis of breast cancer relying on the spatial interaction between tumor-infiltrating lymphocytes and tumors. In In ternational Conference on Medical Image Computing and Computer-Assisted Intervention, pages 612–621. Springer, 2023